Communication: The influence of CO2 poisoning on overvoltages and discharge capacity in non-aqueous Li-Air batteries

Mekonnen, Yedilfana Setarge; Knudsen, Kristian Bastholm; Mýrdal, Jón Steinar Garðarsson; Younesi, Reza; Højberg, Jonathan; Hjelm, Johan; Norby, Poul; Vegge, Tejs

Published in:
Journal of Chemical Physics

Link to article, DOI:
10.1063/1.4869212

Publication date:
2014

Document Version
Publisher's PDF, also known as Version of record

Communication: The influence of CO2 poisoning on overvoltages and discharge capacity in non-aqueous Li-Air batteries

Yedilfana S. Mekonnen, Kristian B. Knudsen, Jon S. G. Mýrdal, Reza Younesi, Jonathan Højberg, Johan Hjelm, Poul Norby, and Tejs Vegge

Citation: The Journal of Chemical Physics **140**, 121101 (2014); doi: 10.1063/1.4869212
View online: http://dx.doi.org/10.1063/1.4869212
View Table of Contents: http://scitation.aip.org/content/aip/journal/jcp/140/12?ver=pdfcov
Published by the AIP Publishing

Communication: The influence of CO_2 poisoning on overvoltages and discharge capacity in non-aqueous Li-Air batteries

Yedilfana S. Mekonnen,[1,2] Kristian B. Knudsen,[1] Jon S. G. Mýrdal,[1] Reza Younesi,[1] Jonathan Højberg,[1] Johan Hjelm,[1] Poul Norby,[1] and Tejs Vegge[1,a)]
[1]*Department of Energy Conversion and Storage, Technical University of Denmark, Frederiksborgvej 399, DK-4000 Roskilde, Denmark*
[2]*Center for Atomic-scale Materials Design, Technical University of Denmark, DK-2800 Lyngby, Denmark*

(Received 31 January 2014; accepted 11 March 2014; published online 24 March 2014)

The effects of Li_2CO_3 like species originating from reactions between CO_2 and Li_2O_2 at the cathode of non-aqueous Li-air batteries were studied by density functional theory (DFT) and galvanostatic charge-discharge measurements. Adsorption energies of CO_2 at various nucleation sites on a stepped $(1\bar{1}00)$ Li_2O_2 surface were determined and even a low concentration of CO_2 effectively blocks the step nucleation site and alters the Li_2O_2 shape due to Li_2CO_3 formation. Nudged elastic band calculations show that once CO_2 is adsorbed on a step valley site, it is effectively unable to diffuse and impacts the Li_2O_2 growth mechanism, capacity, and overvoltages. The charging processes are strongly influenced by CO_2 contamination, and exhibit increased overvoltages and increased capacity, as a result of poisoning of nucleation sites: this effect is predicted from DFT calculations and observed experimentally already at 1% CO_2. Large capacity losses and overvoltages are seen at higher CO_2 concentrations. © *2014 AIP Publishing LLC*. [http://dx.doi.org/10.1063/1.4869212]

I. INTRODUCTION

As energy storage needs are growing rapidly, there is also an increase in research into high energy density materials for energy storage. Significant attention has been given to metal-air batteries, particularly Li-air batteries, as future environmentally friendly high energy density storage for vehicles, where the capacity offered by existing Li-ion technology is too low to solve the increasing demands on batteries.[1] The Li-O_2 couple is particularly attractive and could have ∼5–10 times greater specific energies than currently available Li-ion batteries, though there are severe scientific and technical challenges that need to be addressed.[2,3] Such as a clear understanding of the Li_2O_2 growth mechanisms, transport processes, interfacial phenomena, air impurities, and stability of the key components are vital parts of non-aqueous rechargeable Li-air cell research.[4]

As first reported by Abraham and Jiang in 1996, the Li-O_2 battery with aprotic solvent is shown to be rechargeable, when Li_2O_2 is formed during discharge at the cathode.[5] Detailed understanding of the Li_2O_2 growth mechanism is important to solve the problem associated with the practical limitations of the battery. Previous theoretical works by Hummelshøj *et al.*[6] and Radin *et al.*[7,8] showed that steps on a reconstructed $(1\bar{1}00)$surface could act as nucleation sites for low discharge overvoltage and facets such as (0001), $(1\bar{1}00)$, and $(11\bar{2}0)$ have similar surface energies. Hummelshøj *et al.*[9] have also shown that surfaces are potential dependent and vary during discharge and charge. According to G_0W_0 calculations, both Li_2O_2 and Li_2CO_3 are insulating materials with wide band gap of 4.9 and 8.8 eV, respectively.[10–12] Therefore, as these materials deposit at the cathode surface during discharge they will limit the electronic conduction and lead to sudden death during discharge within 5–10 nm thick Li_2O_2 deposits.[13,14] However, recent DFT calculations found that hole and electron polaronic transports at the surface and in bulk Li_2O_2 and Li_2CO_3 can take place. Using a PBE+U (Hubbard-corrected Perdew–Burke–Ernzerhof) exchange correlation functional, Garcia-Lastra *et al.*[11] revealed that the hole polarons have higher mobility than electron polarons and Li_2CO_3 exhibits lower conduction than Li_2O_2. Recent works by Luntz *et al.* have shown that hole tunneling should dominate and polaronic transport is only expected to be significant in Li_2O_2 at elevated temperatures and low current densities.[15,16]

Li_2CO_3 like crystalline species are formed by parasitic side reactions between the Li_2O_2 or LiO_2 and carbon sources from air impurities such as CO and CO_2 gases,[17] the graphite itself, or the decomposition of aprotic electrolytes. Younesi *et al.*[18,34] reported the degradation of various electrolytes by Li_2O_2 and documented Li_2CO_3 as a decomposition product from aprotic electrolytes. Likewise, McCloskey *et al.*[3] have shown that carbonates accumulate at the C-Li_2O_2 and Li_2O_2-electrolyte interfaces and are responsible for a large potential increase during recharge and a huge decrease in exchange current density. This makes growth of Li_2O_2 on Li_2CO_3 an equally important process to investigate, but this is beyond the scope of this communication. As reported by Siegfried *et al.*[19] and Myrdal and Vegge[20] adsorption of sulfur containing compounds on oxide surfaces could also control the electrochemical growth mechanism. Adsorbed species at surfaces can potentially block the nucleation sites, and therefore, alter the growth directions, overvoltages, and capacities.

In this communication, we address the influence of CO_2 contamination on the Li_2O_2 growth mechanism, discharge/charge overvoltages, and capacity in non-aqueous

a)E-mail: teve@dtu.dk

TABLE I. Adsorption energies of CO_2 in the gas phase at $(1\bar{1}00)$ Li_2O_2 surface.

Species	Sites	Adsorption energy (eV)
CO_2	Step valley	−0.73
	Terrace valley	−0.21
	Step ridge	−0.02

Li-air batteries using density functional theory (DFT) and galvanostatic measurements. Among other air contaminants, CO_2 is the most critical subject due to its high solubility in aprotic electrolytes and high reactivity with Li_2O_2 to form an insulating material Li_2CO_3.

II. COMPUTATIONAL RESULTS AND ANALYSIS

DFT[21–23] as implemented in the GPAW (grid-based projector-augmented wave method) code[24] is used to perform the presented calculations through the atomic simulation environment (ASE).[25] GPAW is built on real space grids and non-valence electrons are described by PAW (projector augmented-wave method).[26,27] Electron exchange and correlation is approximated by the revised Perdew–Burke–Ernzerhof (RPBE) functional.[28] The stepped $(1\bar{1}00)$ Li_2O_2 surface with a super cell consisting of a 56–64 atoms slab with a 18 Å vacuum layer between periodic images along the z-axis, see Fig. S1 in the supplementary material.[35] Since the oxygen rich (0001) facet will also be exposed, in particular under charging conditions,[9] and subsequent investigations should be performed to analyze the detailed mechanisms of CO_2 bonding to this facet. Recent computational DFT results for SO_2 adsorption on stepped (0001) and $(1\bar{1}00)$ surfaces do, however, show preferential bonding to the $(1\bar{1}00)$ facets,[20] which is investigated here. The k-points are sampled with a (4,4,1) Monkhorst-Pack mesh and 0.15 grid points is used. Atomic energy optimization calculations are performed until all forces are less than 0.01 eV/Å. Energy barriers are calculated by the climbing image nudged elastic band (CINEB) method.[29–31]

Adsorption energies of CO_2 at various nucleation sites on a stepped $(1\bar{1}00)$ Li_2O_2 surface were determined, see Table I. CO_2 binds preferentially at the step valley site and weakly binds at the step ridge site. NEB calculations show that once CO_2 is adsorbed at step valley site, it is bound by barriers upwards of 3 eV, see Fig. S2 in the supplementary material,[35] since the CO_2 molecule is required to desorb from the surface prior to re-adsorbing at the step site. The detailed nature of a conversion of adsorbed CO_2 to Li_2CO_3 warrants further investigations, but we find the adsorption of a single CO_2 molecule forms a $Li_{\sim 3}CO_3$-type complex (Fig. 1(b)), which could act as a nucleation site for further growth of Li_2CO_3.

The computational lithium electrode approach is used in the free energy calculations.[6,32] Defined as, U = 0, when bulk Li anode and Li ions in solution ($Li^+ + e^-$) are at equilibrium. The free energy change of the reaction is shifted by $-neU$ at an applied bias, where n is the number of transferred electrons; other assumptions are listed in the supplementary material.[35] As reported by Hummelshøj *et al.*, kinks and steps sites of the stepped $(1\bar{1}00)$ Li_2O_2 surface are favorable nucleation sites for a low overvoltage Li_2O_2 growth mechanism. The influence of CO_2 poisoning on the Li_2O_2 growth mechanism is studied while CO_2 is already adsorbed at step valley site (Fig. 1(b)).

The free energy diagram in Fig. 2 shows a four steps, two formula units Li_2O_2 growth mechanism on the stepped $(1\bar{1}00)$ Li_2O_2 surface with and without CO_2. The first step in the presence of CO_2 is adsorption of LiO_2 species (Fig. 1(c)), and which reduces the binding energy by 0.44 V compared to the pure discharge. The next step is the addition of a second LiO_2 species (Fig. 1(d)), which is the potential limiting charge step that raises the binding energy by 0.20 V compared to pure Li_2O_2. This is followed by subsequent additions of two Li (Figs. 1(e) and 1(f)) with relatively small binding energies with respect to a pure discharge. In the pure O_2 discharge mechanism, unlike in the presence of CO_2, addition of the first Li is the limiting charge potential step. The $2Li_2O_2$ growth at the step surface effectively displaces CO_2 from the step to the less stable terrace site.

Hummelshøj *et al.* have reported that the pure Li_2O_2 growth mechanism follows a 4 steps reaction mechanism, where all reaction steps are electrochemical, similar to what is seen in the presence of CO_2. The equilibrium potential can be obtained as $U_0 = -\Delta G/2e$. The effective equilibrium potential on a pure surface becomes 2.73 V (experimental value, $U_{0,Exp} = 2.85$ V), while in the presence of CO_2, this is effectively reduced to 2.53 V for the first cycle due to the shift in binding energy of CO_2 from a step valley to terrace site. As a result, discharge at other facets may become activate.[9] At neutral bias all reaction steps are downhill, but at an applied potential, the free energy difference changes for each step calculated as

$$\Delta G_{i,U} = \Delta G_i - eU. \quad (1)$$

The lowest free energy step, $\Delta G_{i,min}$, along the reaction path becomes uphill first at an applied potential called limited discharge potential, $U_{discharge}$, while the largest free energy step, $\Delta G_{i,max}$, that is last to become downhill for the reversed reaction at an applied potential called limited charge potential, U_{charge}, obtained as

$$U_{discharge} = \min[-\Delta G_i/e] \text{ and } U_{charge} = \max[-\Delta G_i/e]. \quad (2)$$

In the presence (absence) of a single CO_2 molecule, this discharge occurs as described in Fig. 1, resulting in $U_{discharge}$ = 2.21 V (2.66 V), and U_{charge} = 2.97 V (2.81 V) and the discharge and charge overvoltages in the presence (absence) of CO_2 are $\eta_{discharge} = 0.31$ V (0.07 V), and $\eta_{charge} = 0.44$ V (0.08 V). The calculated 0.44 V overvoltage for charge corresponds to low CO_2 concentrations, where only a single CO_2 molecule is adsorbed on the Li_2O_2 step forming a $Li_{\sim 3}CO_3$ type complex (see Fig. 1). Here, the charging process follows the same reaction steps as the discharge, but in reverse (from right to left in Fig. 2), i.e., the first two steps are desorption of two Li and followed by desorption of 2 LiO_2 species: in total desorbing 2 Li_2O_2 units from the surface and returning to the configuration in Fig. 1(b). Quantitative agreement with

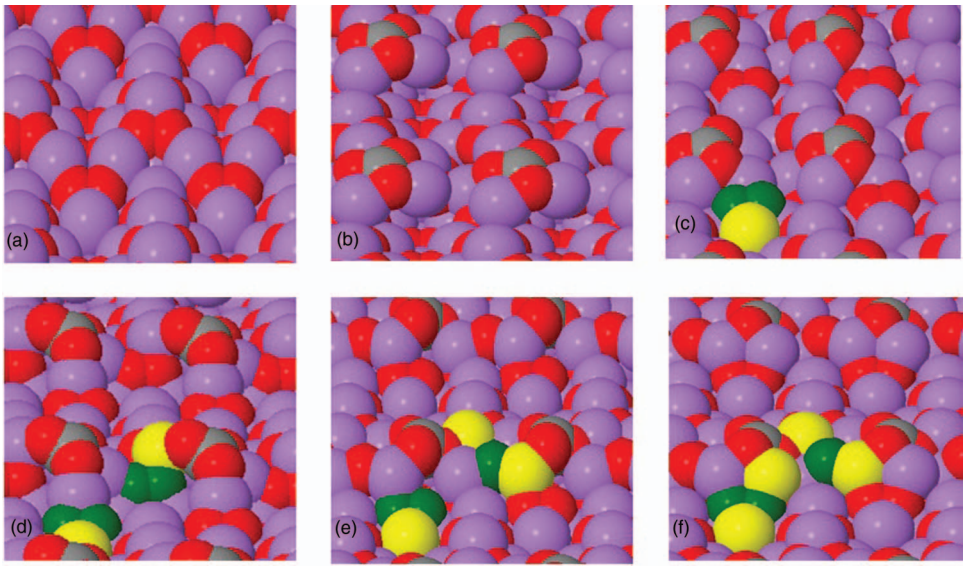

FIG. 1. Stepped Li_2O_2 ($1\bar{1}00$) surface before and after adsorption of CO_2 and 4 steps Li_2O_2 growth pathways during discharge. (a) Pure stepped Li_2O_2 surface. (b) CO_2 adsorbs to step valley site forming a $Li_{\sim 3}CO_3$ type complex. (c) 1st LiO_2 adsorbs. (d) 2nd LiO_2 adsorbs. (e) 1st Li. (f) 2nd Li adsorbs to the surface completing growth of 2 Li_2O_2 formula units. Atoms labeled as: C (gray), Li (purple), and O (red). Deposited atoms shown as: Li (yellow) and O (green).

experimental overvoltages can therefore only be expected for low concentrations of CO_2 (e.g., 1%). For higher CO_2 concentrations, the formation of crystalline Li_2CO_3 would be expected, resulting in significantly larger overvoltages.[3]

III. EXPERIMENTAL RESULTS AND ANALYSIS

Li-air batteries were constructed using a Swagelok design and assembled inside an Ar-filled glovebox ($\leq$3 ppm O_2 and H_2O). Each battery contained a 200 μl 1 M LiTFSI (99.95%, Sigma-Aldrich) and 1,2-dimethoxymethane, DME, (H_2O < 20 ppm, BASF) electrolyte. Cathodes consisted of P50 AvCarb carbon paper (Fuel cell store), which were sonicated using 2-propanol (99.5%, Sigma-Aldrich) and acetone ($\geq$99.8%, Sigma-Aldrich), introduced into a glovebox where they were rinsed with DME before drying in vacuum at 80 °C for 12 h. Cathodes were supported by a 316 steel mesh. A 10 mm diameter lithium foil (99.9%, Sigma-Aldrich) was used as anode. Two Celgard separators 2500 (Celgard) were placed in between the two electrodes. The separators were sonicated in EtOH (99.9%, Sigma-Aldrich), transferred to a glovebox, and rinsed with DME before drying in vacuum at 80 °C for 12 h. Experiments were performed using a Bio-Logic VMP3 Multichannel galvanostat (Bio-Logic, Claix, France). Batteries were operated in two galvanostatic modes: First, at 100 μA (127.3 μA/cm^2) where cells were discharged to 2 V and charged to 4.6 V vs. Li^+/Li. Second, at 50 μA (63.6 μA/cm^2) using the same potential limits.

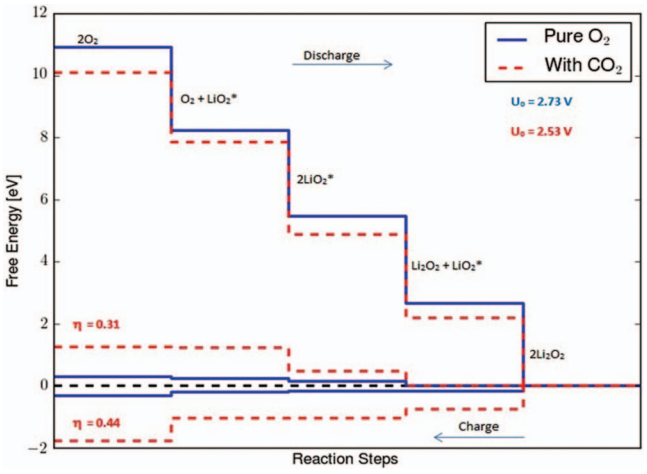

FIG. 2. Calculated free energy diagrams for a four steps discharge mechanism on a stepped ($1\bar{1}00$)Li_2O_2 surface with and without adsorbed CO_2.

To investigate the effect of gaseous CO_2, the assembled cells were purged with three different atmospheres: 0/100 CO_2/O_2, 1/99 CO_2/O_2, and 50/50 CO_2/O_2. Three individual batteries were assembled and investigated for each atmosphere and each curve presented in Figs. 3 and 4 is therefore an average of three cells with the equal atmosphere as shown in Fig. S3 in the supplementary material.[35] The lowest discharge capacity was observed for the 50% CO_2 cells and is likely caused by the high concentration of electrochemically inactive CO_2. A similar effect was observed, by Gowda *et al.*[17] for a pure CO_2 cell, where the cell potential immediately dropped. It should however be noted that Takechi *et al.*[33] observed, quite to the contrary of our observations, higher discharge capacities up to 70% CO_2 with respect to pure O_2 cells. Interestingly, a higher discharge capacity was observed for the 1% CO_2 cells in respect to the pure O_2 cells as shown in Fig. 3 (inset). A possible explanation is the dissolution of Li_2CO_3 species in DME and/or, as also suggested by Gowda *et al.*, or a change in deposition morphology compared to that deposited in the pure O_2 cells as suggested by Myrdal and Vegge.[20] Such morphological changes could increase the total electrodeposited layer and lead to higher capacities.

All CO_2 cells have higher discharge overvoltages compared to cells with pure O_2 at a discharge rate of 127.3 μA/cm^2, which may be caused by the blocking of the

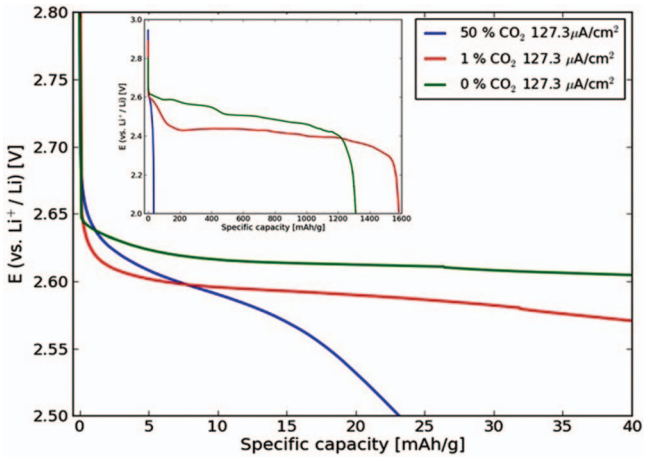

FIG. 3. Galvanostatic discharge profiles at 127.3 μA/cm^2 discharge at three different atmospheres: 50% CO_2, 1% CO_2, and 0% CO_2. Inset shows the increase in discharge capacity in 1% CO_2.

active nucleation sites by solubilized CO_2, forcing the reactions to follow pathways with higher overvoltages. This effect can even be seen at 1% CO_2, as illustrated in Fig. 3 above. The charge capacity, as seen in Fig. 4 and Fig. S4 in the supplementary material,[35] is very dependent on the CO_2 concentration, with high concentrations limiting charge capacity and thereby the cell reversibly. The 50% CO_2 cells reach the lower potential limit (2.0 V) early, at approximately 35 mAh/g, while 1% CO_2 cells and pure O_2 cells continued until capacities in the range 1150–1600 mAh/g were reached depending on current density. The low charge capacity at high CO_2 contaminations should be attributed to the poor Li-CO_2 electrochemistry, also reported by Gowda *et al.* The charging overvoltages are a function of both current density and the level of CO_2 contamination. While there is no significant difference in overvoltages between cells charge at 127.3 and 63.6 μA/cm^2 for 50% CO_2 cells, which again can be attributed to the poor Li-CO_2 electrochemistry. At 127.3 μA/cm^2, there is an increase in overvoltage of about 0.4 and 0.3 V for 1% CO_2 cells and 0% CO_2 cells, respectively. The general increase in overvoltages with increasing current density can be explained

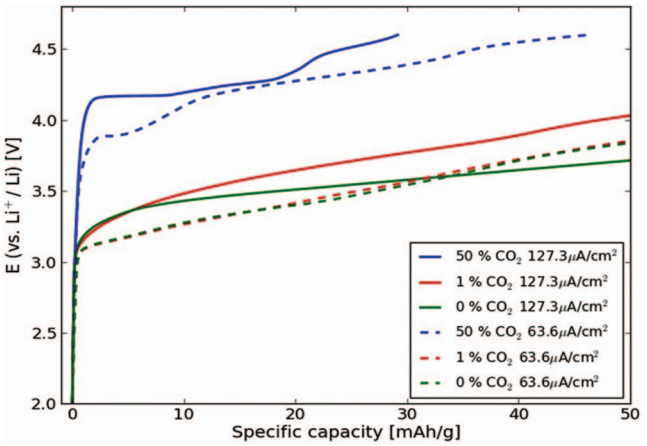

FIG. 4. Galvanostatic charge profiles at 127.3 (solid) and 63.6 (dotted) μA/cm^2 at three different atmospheres: 50% CO_2, 1% CO_2, and 0% CO_2.

by the Butler-Volmer model, while the larger overvoltage for the 1% CO_2 cells than 0% CO_2 cells is expectedly caused by the formation and oxidation of the carbonate like species (Fig. 1(b)). A second charge at 63.6 μA/cm^2 shows identical results for 1% and 0% CO_2. This can be ascribed to the evolution of CO_2 observed during the initial charge cycle, where CO_2 is released at 4.5 V, as shown in Fig. S5 in the supplementary material,[35] resulting in residual CO_2 in the electrolyte causing blocking of the step sites in subsequent charging experiments.

IV. CONCLUSIONS

Influences of CO_2 poisoning at a stepped (1$\bar{1}$00) Li_2O_2 surface in non-aqueous Li-air battery were studied using DFT calculations and cells were characterized by electrochemical charge-discharge measurements. CO_2 preferentially binds at step valley site at the Li_2O_2 surface and the Li_2O_2 growth mechanism consists of four electrochemical steps, following the same sequence for both pure and contaminated systems. Accordingly, the first step of the growth mechanism is the adsorption of two LiO_2 species and followed by addition of two Li to form 2 Li_2O_2 at the cathode surface. For charge in the low CO_2 limit, a similar reaction will occur, but in reverse order.

Low concentrations of CO_2 (1%) effectively block the surface-active nucleation sites and alter the shape and growth directions of Li_2O_2 on the surface; resulting in an increased capacity of the battery at the expense of an increase in the overvoltage in the presence of CO_2. A similar behavior is seen in pure oxygen following charging to 4.5 V, resulting from decomposition reactions. The effective discharge potential is reduced by 0.20 V on a stepped (1$\bar{1}$00) Li_2O_2 surface, shifting the reaction to alternate nucleation sites. In general, the DFT calculations and experimental results show that the recharging process is strongly influenced by CO_2 contamination, and exhibits significantly increased charging overvoltage, which is observed already with 1% CO_2 contamination, while at 50% CO_2 a large capacity loss is also seen.

ACKNOWLEDGMENTS

The authors acknowledge support of this work from the ReLiable project (Project No. 11-116792) funded by the Danish Council for Strategic Research Programme Commission on Sustainable Energy and Environment.

[1]D. Linden and T. Reddy, *Hand Book of Batteries*, 3rd ed. (McGraw Hill, New York, 2001).
[2]T. Ogasawara, A. Débart, M. Holzapfel, P. Novák, and P. G. Bruce, J. Am. Chem. Soc. **128**, 1390 (2006).
[3]B. D. McCloskey, A. Speidel, R. Scheffler, D. C. Miller, V. Viswanathan, J. S. Hummelshøj, J. K. Nørskov, and A. C. Luntz, J. Phys. Chem. Lett. **3**, 997 (2012).
[4]G. Girishkumar, B. D. McCloskey, A. C. Luntz, S. Swanson, and W. Wilcke, J. Phys. Chem. Lett. **1**, 2193 (2010).
[5]K. M. Abraham and Z. Jiang, J. Electrochem. Soc. **143**, 1 (1996).
[6]J. S. Hummelshøj, J. Blomqvist, S. Datta, T. Vegge, J. Rossmeisl, K. S. Thygesen, A. C. Luntz, K. W. Jacobsen, and J. K. Nørskov, J. Chem. Phys. **132**, 071101 (2010).
[7]M. D. Radin, J. F. Rodriguez, F. Tian, and D. J. Siegel, J. Am. Chem. Soc. **134**, 1093 (2011).

[8]M. D. Radin, F. Tian, and D. J. Siegel, J. Mat. Sci. **47**, 7564 (2012).
[9]J. S. Hummelshøj, A. C. Luntz, and J. K. Nørskov, J. Chem. Phys. **138**, 034703 (2013).
[10]P. Albertus, G. Girishkumar, B. D. McCloskey, R. S. Sanchez-Carrera, B. Kozinsky, J. Christensen, and A. C. Luntz, J. Electrochem. Soc. **158**(3), A343 (2011).
[11]J. M. Garcia-Lastra, J. S. G. Myrdal, K. S. Thygesen, and T. Vegge, J. Phys. Chem. C **117**, 5568 (2013).
[12]J. M. Garcia-Lastra, J. D. Bass, and K. S. Thygesen, J. Chem. Phys. **135**, 121101 (2011).
[13]V. Viswanathan, K. S. Thygesen, J. S. Hummelshøj, J. K. Nørskov, G. Girishkumar, B. D. McCloskey, and A. C. Luntz, J. Chem. Phys. **135**, 214704 (2011).
[14]J. Chen, J. S. Hummelshøj, K. S. Thygesen, J. S. G. Myrdal, J. K. Nørskov, and T. Vegge, Catal. Today **165**, 2 (2011).
[15]J. B. Varley, V. Viswanathan, J. K. Nørskov, and A. C. Luntz, Energy Environ. Sci. **7**, 720 (2014).
[16]A. C. Luntz, V. Viswanathan, J. Voss, J. B. Varley, J. K. Nørskov, R. Scheffler, and A. Speidel, J. Phys. Chem. Lett. **4**, 3494 (2013).
[17]S. R. Gowda, A. Brunet, G. M. Wallraff, and B. D. McCloskey, J. Phys. Chem. Lett. **4**, 276 (2013).
[18]R. Younesi, M. Hahlin, F. Björefors, P. Johansson, and K. Edström, Chem. Mater. **25**, 77 (2013).
[19]M. J. Siegfried and K. S. Choi, Adv. Mat. **16**, 1743 (2004).
[20]J. S. G. Myrdal and T. Vegge, "DFT study of selective poisoning of Li-Air batteries for increased discharge capacity," RSC Adv. (to be published).
[21]P. Hohenberg and W. Kohn, Phys. Rev. **136**, B864 (1964).
[22]W. Kohn and L. Sham, Phys. Rev. **140**, A1133 (1965).
[23]J. J. Mortensen, L. B. Hansen, and K. W. Jacobsen, Phys. Rev. B **71**, 035109 (2005).
[24]J. Enkovaara, C. Rostgaard, J. J. Mortensen, J. Chen, M. Dulak, L. Ferrighi, J. Gavnholt, C. Glinsvad, V. Haikola, H. A. Hansen, H. H. Kristoffersen, M. Kuisma, A. H. Larsen, L. Lehtovaara, M. Ljungberg, O. Lopez-Acevedo, P. G. Moses, J. Ojanen, T. Olsen, V. Petzold, N. A. Romero, J. Stausholm-Moller, M. Strange, G. A. Tritsaris, M. Vanin, M. Walter, B. Hammer, H. Hakkinen, G. K. H. Madsen, R. M. Nieminen, J. K. Nørskov, M. Puska, T. T. Rantala, J. Schiøtz, K. S. Thygesen, and K. W. Jacobsen, J. Phys. Condens. Matter **22**, 253202 (2010).
[25]S. R. Bahn and K. W. Jacobsen, Comput. Sci. Eng. **4**, 56 (2002).
[26]P. E. Blöchl, Phys. Rev. **50**, 17953 (1994).
[27]P. E. Blöchl, C. J. Först, and J. Schimpl, Bull. Mater. Sci. **26**, 33 (2003).
[28]B. Hammer, L. B. Hansen, and J. K. Nørskov, Phys. Rev. B **59**, 7413 (1999).
[29]H. Jonsson, G. Mills, and K. W. Jacobsen, *Classical and Quantum Dynamics in Condensed Phase Systems*, edited by B. J. Berne, G. Cicotti, and D. F. Coker (World Scientific, 1998).
[30]G. Henkelman and H. Jónsson, J. Chem. Phys. **113**, 9978 (2000).
[31]G. Henkelman, B. Uberuaga, and H. A. Jónsson, J. Chem. Phys. **113**, 9901 (2000).
[32]J. K. Nørskov, J. Rossmeisl, A. Logadottir, L. Lindqvist, J. R. Kitchin, T. Bligaard, and H. Jonsson, J. Phys. Chem. B **108**, 17886 (2004).
[33]K. Takechi, T. Shiga, and T. Asaoka, Chem. Commun. **47**, 3463 (2011).
[34]R. Younesi, P. Norby, and T. Vegge, ECS Electrochem. Lett. **3**, A15 (2014).
[35]See supplementary material at http://dx.doi.org/10.1063/1.4869212 for Figs. S1–S5.